EurJIC
European Journal of Inorganic Chemistry

Full Papers
doi.org/10.1002/ejic.202000891

Chemistry Europe
European Chemical Societies Publishing

Tunable Potassium Ion Conductivity and Magnetism in Substituted Layered Ferrates

Ralf Albrecht,[a] Jens Hunger,[a] Markus Hoelzel,[b] Emmanuelle Suard,[c] Walter Schnelle,[d] Thomas Doert,*[a] and Michael Ruck[a, d]

Five substituted oxohydroxoferrates $K_{2-x}(Fe,M)_4O_{7-y}(OH)_y$ (M = Si, Ge, Ti, Mn, Ir) were synthesized in a potassium hydroxide hydroflux with a molar base-water ratio q(K) of about 0.9. While the hexagonal prisms of $K_{2-x}(Fe,Ti)_4O_{7-y}(OH)_y$ crystallize in $P6_3/mcm$, all other compounds form hexagonal plates with the trigonal space group $P\bar{3}1m$. The crystal structure of the oxohydroxoferrates resembles ß-alumina. It consists of honeycomb layers $^2_\infty$ Fe_2O_6] of edge-sharing [FeO_6] octahedra, where the hexagonal voids are capped by vertex-sharing [FeO_4] tetrahedra pairs. The cavities between the oxoferrate layers host the potassium ions. Depending on M, the substitution affects different iron positions and varies between 5 and 20%. The magnetic structures of the antiferromagnetic compounds were determined by neutron powder diffraction. The potassium ion conductivity was characterized by electrochemical impedance spectroscopy at room temperature. By storing the oxohydroxoferrates in air or annealing them at 700 °C the ion conductivity was significantly increased, e.g. to $5.0 \cdot 10^{-3}$ S cm^{-1} for a pressed pellet of the iridium substituted compound.

Introduction

Recently, we synthesized the potassium oxohydroxoferrate $K_{2-x}Fe_4O_{7-x}(OH)_x$ ($x \approx 0.3$)[1] with the hydroflux method, which uses a ultrabasic reaction medium consisting of an approximately equimolar mixture of alkali metal hydroxide and water.[2] In the specific case, we used potassium hydroxide for the hydroflux and $Fe(NO_3)_3 \cdot 9H_2O$ as iron source. The base concentration is one of the most important reaction parameters, as slight changes can cause the formation of different products. With increasing base concentration in the range of the molar base-water ratio $q(K) = n(KOH) : n(H_2O)$ of 0.5 to 1.4, four different phase-pure products were obtained: α-Fe_2O_3, $K_{2-x}Fe_4O_{7-x}(OH)_x$, $K_2Fe_2O_3(OH)_2$, or $KFeO_2$.[3]

$K_{2-x}Fe_4O_{7-x}(OH)_x$ crystallizes in the trigonal space group $P\bar{3}1m$ with $a = 517.5(1)$ pm and $c = 692.3(1)$ pm at 100 K. Its crystal structure resembles ß-alumina (Figure 1). Edge-sharing [FeO_6] octahedra form a honeycomb $^2_\infty$ Fe_2O_6] net. The hexagonal voids of this net are capped on both sides by [FeO_4] tetrahedra, which share vertices with three [FeO_6] octahedra. [FeO_4] tetrahedra of neighboring layers share their apices to form pillar-like linkers between adjacent honeycomb nets. This kind of stacking creates an oxoferrate framework with large interlayer voids where the potassium cations reside. The substoichiometric potassium content is compensated by hydroxide groups, so that every iron in $K_{2-x}Fe_4O_{7-x}(OH)_x$ is trivalent as confirmed by Mößbauer spectroscopy.[1] The [FeO_4] tetrahedra pairs can be arranged in a staggered or an ecliptic configuration, giving rise to different polytypes.[1] The structure motif of $K_{2-x}Fe_4O_{7-x}(OH)_x$ was observed in other oxoferrates, like $BaFe_4O_7$ or $K_{0.22}B_{0.89}Fe_4O_7$,[4] as well as in other classes of material like the high pressure phases $A_2Mg_2Si_2O_7$ (A = Na, K).[5,6]

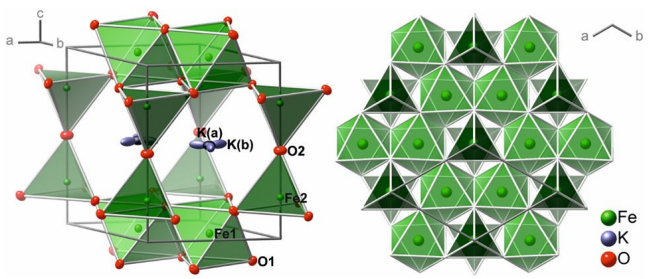

Figure 1. Left: Crystal structure of $K_{2-x}(Fe,M)_4O_{7-y}(OH)_y$ in $P\bar{3}1m$. Ellipsoids enclose 90% of the probability density of the atoms at 100 K. Right: Oxoferrate layer with honeycomb nets of [FeO_6] octahedra (light green) and capping [FeO_4] tetrahedra (dark green).

[a] R. Albrecht, Dr. J. Hunger, Prof. Dr. T. Doert, Prof. Dr. M. Ruck
Faculty of Chemistry and Food Chemistry,
Technische Universität Dresden,
01069 Dresden, Germany
E-mail: thomas.doert@tu-dresden.de
http://chm.tu-dresden.de/ac2/
[b] Dr. M. Hoelzel
Heinz Maier-Leibnitz Zentrum (MLZ),
Technische Universität München,
Lichtenbergstraße 1, 85747 Garching, Germany
[c] Dr. E. Suard
Institut Laue-Langevin,
71 Avenue des Martyrs,
38042 Grenoble, France
[d] Dr. W. Schnelle, Prof. Dr. M. Ruck
Max-Planck Institute for Chemical Physics of Solids
Nöthnitzer Staße 40, 01187 Dresden, Germany

Supporting information for this article is available on the WWW under https://doi.org/10.1002/ejic.202000891

Upon heating $K_{2-x}Fe_4O_{7-x}(OH)_x$, the potassium ions order into a $2a \times 2b$ superstructure with empty and fully occupied K sites, before, at higher temperature, a topotactical transformation into $K_{1+x}Fe_{11}O_{17}$ (β-/β''-aluminate type) and finally the thermal decomposition to Fe_2O_3 occurs.[1]

Magnetic measurements revealed antiferromagnetic ordering in $K_{2-x}Fe_4O_{7-x}(OH)_x$. The Néel temperature T_N could not be determined because thermal decomposition of the compounds starts before T_N is reached. Neutron diffraction confirmed the antiferromagnetic ordering of the iron-centered magnetic moments within the tetrahedra pairs and between [FeO_4] tetrahedra and adjacent [FeO_6] octahedra. All moments are aligned parallel to the *c* axis and have the same orientation for all iron atoms with the same *z* parameter.[1]

In this contribution, we address the question whether the substitution of iron(III) with magnetically active, *M* = Mn, Ir, and inactive, *M* = Si, Ge, Ti, cations changes the magnetic coupling between the pillared honeycomb layers and possibly generates magnetic frustration. We synthesized various compounds $K_{2-x}(Fe,M)_4O_{7-y}(OH)_y$ and studied their crystal structures and their magnetic properties, the latter by magnetization and neutron scattering experiments. In addition, we report the potassium ion conductivity of these compounds, inspired by the recently published oxoferrate "$K_2Fe_4O_7$" with a similar structure, which was reported to have a higher ion conductivity than any other solid electrolyte used in batteries.[7]

Results and Discussion

Synthesis

The hydroflux method utilizes strongly alkaline media to generate a unique reaction environment with moderate temperatures. It is a hybrid approach between the aqueous hydrothermal synthesis and the molten hydroxide flux technique. These novel reaction conditions facilitated new discoveries even in systems that had been studied extensively over many decades. The advantages of a hydroflux system are the relatively low reaction temperatures, the pressure-less setup, the high crystallinity of the products, and the good solubility of various oxides and hydroxides.[8]

For the syntheses of the substituted potassium oxohydroxoferrates $K_{2-x}(Fe,M)_4O_{7-y}(OH)_y$ (*M* = Si, Ge, Ti, Mn, Ir), we used a stainless steel autoclave with a PTFE inlet, which is needed due to the highly corrosive medium and the required constant water content (i.e. base concentration), although almost no pressure was generated during the reaction.[9] As observed in the synthesis of $K_{2-x}Fe_4O_{7-x}(OH)_x$, a reaction time of 10 h and a temperature of 200 °C are sufficient to obtain a phase-pure, highly crystalline product with single-crystals of about 250 µm (Figure 2).[1] Longer reaction times promote the decomposition of the oxohydroxoferrates into α-Fe_2O_3 (hematite). First hematite reflections were observed in powder X-ray diffraction patterns (PXRD) of products obtained with reaction times of 50 h, phase-pure hematite results if the reaction time exceeds 100 h.

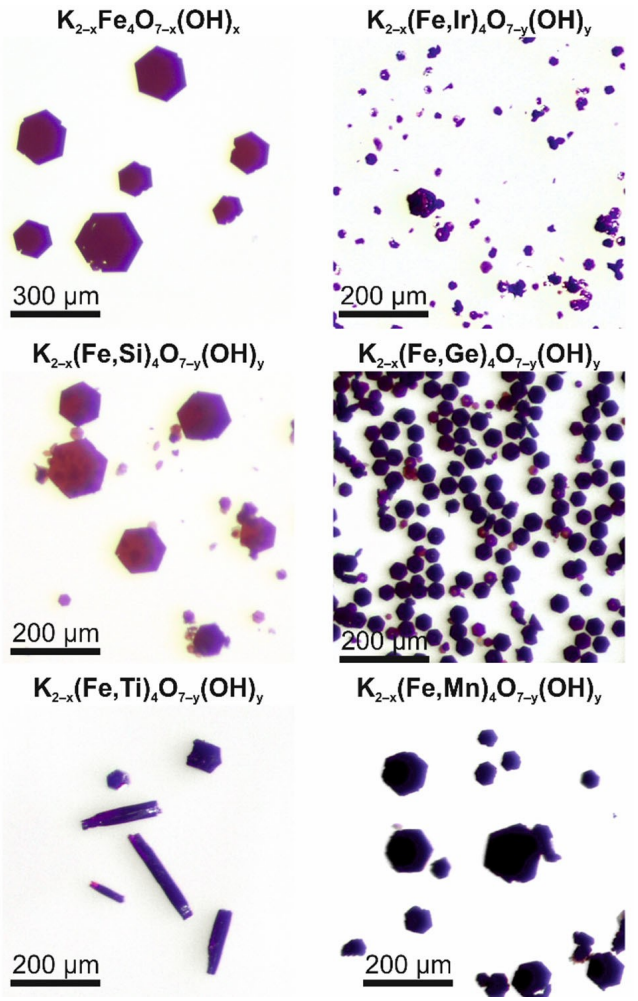

Figure 2. Crystals of $K_{2-x}(Fe,M)_4O_{7-y}(OH)_y$ (*M* = Si, Ge, Ti, Mn, Ir) and the unsubstituted potassium oxohydroxoferrate. Yellow or blue shades around some crystals are caused by the camera setup.

To produce a sufficient amount of these materials for neutron diffraction experiments in a reasonable time, the batches had a theoretical yield of about 8 g of the target compound, i.e. about 25 times more than in the previous syntheses of the unsubstituted oxohydroxoferrate. Moreover, up-scaling of the synthesis required a readjustment of the base-water ratio *q*(K). Instead of the potassium hydroxide-water ratio *q*(K) = 0.7, which we found appropriate for the synthesis of 0.3 g of $K_{2-x}Fe_4O_{7-x}(OH)_x$, the larger batch sizes and reaction volumes needed *q*(K) = 0.9. Conversely, these changed conditions applied to a small batch yielded inhomogeneous reaction products. The properties of each of the substituted compounds presented here were measured on samples from the same batch. The chemical composition of each compound, as discussed below, is given in Table 1. For simplicity we will use the general formula $K_{2-x}(Fe,M)_4O_{7-y}(OH)_y$ throughout this manuscript.

In the following, we will briefly outline the synthesis procedures and specifics for individual compounds. In all syntheses, $Fe(NO_3)_3$ was used as iron source, SiO_2, GeO_2, TiO_2,

Table 1. Results of the energy-dispersive X-ray spectroscopy (EDX), inductively coupled plasma optical emission spectrometry (ICP-OES) and carrier gas hot extraction (CGHE) measurements of the potassium oxohydroxoferrates $K_{2-x}(Fe,M)_4O_{7-y}(OH)_y$ (M = Si, Ge, Ti, Mn, Ir). The listed values for each element were scaled to "Fe + M = 4" in the sum formula $K_{2-x}(Fe,M)_4O_7$. EDX analyses of several crystals were averaged. The standard deviations (in brackets) do not include systematic errors.

$K_{2-x}(Fe,M)_4O_{7-y}(OH)_y$	Si	Ge smooth	Ge flower-like	Ti	Mn thin	Mn rough-1	Mn rough-2	Ir
EDX								
K	1.67(3)	1.51(2)	1.5(1)	1.58(4)	1.14(6)	1.38(2)	1.57(8)	1.27(5)
Fe	3.78(8)	3.71(4)	3.6(3)	3.49(9)	3.2(1)	3.34(3)	3.59(9)	3.69(9)
M	0.22(2)	0.29(2)	0.45(2)	0.51(5)	0.85(7)	0.66(2)	0.41(4)	0.31(3)
O	7.02(9)	7.82(5)	7.7(4)	7.9(1)	7.6(2)	7.00(5)	7.7(1)	7.7(1)
x	0.33(3)	0.49(2)	0.5(1)	0.42(4)	0.86(6)	0.63(2)	0.43(8)	0.73(5)
ICP-OES								
K	1.63(1)	1.54(1)		1.49(3)	1.20(1)			1.31(1)
Fe	3.83(1)	3.93(1)		3.63(4)	3.34(2)			3.73(3)
M	0.17(1)	0.07(1)		0.37(1)	0.66(1)			0.27(1)
CGHE/wt.–% H	0.10(1)	0.14(1)		0.13(1)	0.11(1)			0.21(1)

$Mn(NO_3)_2$, or $IrCl_3$ as starting materials for the *M* element. After the reaction, the product was quickly washed with deionized water until pH neutrality and then stored under argon to prevent decomposition, as had been observed for $K_{2-x}Fe_4O_{7-x}(OH)_x$.[1] Each product was checked by PXRD for its purity and with a standard optical microscope for its morphology as the oxohydroxoferrates usually form well shaped hexagonal plates. In the case of $K_{2-x}(Fe,\mathbf{Ti})_4O_{7-y}(OH)_y$, hexagonal prismatic rods were found in addition (Figure 2).

In first attempts to synthesize $K_{2-x}(Fe,\mathbf{Si})_4O_{7-y}(OH)_y$, an equimolar ratio of iron and silicon was used, which resulted in a red amorphous powder. By lowering the silicon-iron ratio to 0.2, the formation of red powder could be suppressed and a phase-pure crystalline product was obtained. The washed product contained some crystals with a maximum edge length of 150 μm, whereas most crystals had a size of about 30 μm. Overall, the crystals were well-shaped thin hexagonal plates. SiO_2 (and GeO_2 as well) is well soluble in alkaline solutions. We assume that by using high amounts of SiO_2, a metastable intermediate is formed whereas the excess of SiO_2 remains dissolved in the reaction mixture and is eliminated during the washing procedure.

In the synthesis of $K_{2-x}(Fe,\mathbf{Ge})_4O_{7-y}(OH)_y$, starting with the equimolar ratio of germanium and iron yielded a phase-pure product. The crystals of $K_{2-x}(Fe,\mathbf{Ge})_4O_{7-y}(OH)_y$ show a narrow size distribution around 50 μm and have the largest ratio of height to basal edge length of the hexagonal plates excluding those of the titanium compound.

For the synthesis of $K_{2-x}(Fe,\mathbf{Mn})_4O_{7-y}(OH)_y$, we obtained a phase-pure product with a manganese-iron ratio of 0.2. The crystals of the manganese-substituted sample often form truncated or intergrown hexagonal plates. Even thin crystals have black color.

The synthesis of $K_{2-x}(Fe,\mathbf{Ti})_4O_{7-y}(OH)_y$ was more challenging because TiO_2 is by far less soluble in the hydroflux medium than the other starting materials. Experiments with titanium-iron ratios between 0.25 and 1.0 as well as attempts to predissolve TiO_2 by heating 10 h to 250 °C, followed by adding $Fe(NO_3)_3$ failed. Instead, an amorphous orange powder was obtained. We succeeded to synthesis a phase-pure sample of $K_{2-x}(Fe,\mathbf{Ti})_4O_{7-y}(OH)_y$ with a titanium-iron ratio of 0.2 and by increasing the reaction temperature to 250 °C. The red crystals of the titanium-substituted phase form hexagonal columns with lengths up to 250 μm.

For the synthesis of $K_{2-x}(Fe,\mathbf{Ir})_4O_{7-y}(OH)_y$, we used an iridium-iron ratio of 0.1. A larger ratio was not tested, as only a small fraction of the available iridium was incorporated in the product. Iridium(III) is known to be rapidly oxidized to iridium (IV) under basic conditions.[10] The grey crystals of $K_{2-x}(Fe,\mathbf{Ir})_4O_{7-y}(OH)_y$ are the smallest and thinnest of our substitution series. The size distribution was similar to the one observed for the silicon substitution.

Chemical composition

A scanning electron microscope (SEM) provided more detailed images of the crystals (Figure 3). Additionally, energy-dispersive X-ray spectroscopy (EDX) and inductively coupled plasma optical emission spectrometry (ICP-OES) were used to determine the composition of crystals of the substituted samples (Table 1). As the unsubstituted potassium oxohydroxoferrate slowly decomposes in air and forms potassium carbonate on the surface,[1] samples of all oxohydroxometalates were exposed to ambient air for more than a month and then re-analyzed with SEM and EDX. Remarkably, only the germanium and titanium containing compounds showed visible signs of decomposition in air. The tiny white crystals that formed on the surface of the dark colored metalate crystals had high carbon and potassium contents, indicating the segregation of potassium hydroxide, which then absorbs carbon dioxide from the air to form potassium carbonate. In contrast, none of the crystals stored under argon showed decomposition even after more than one year.

For $K_{2-x}(Fe,\mathbf{Si})_4O_{7-y}(OH)_y$ a silicon-iron ratio of about 5 % was measured, which is four times lower than the ratios of the respective starting materials. The standard deviation in the determination of the iron and silicon content received from EDX measurements are relatively high due to concentration gradients found in the crystals: EDX line scans recorded over

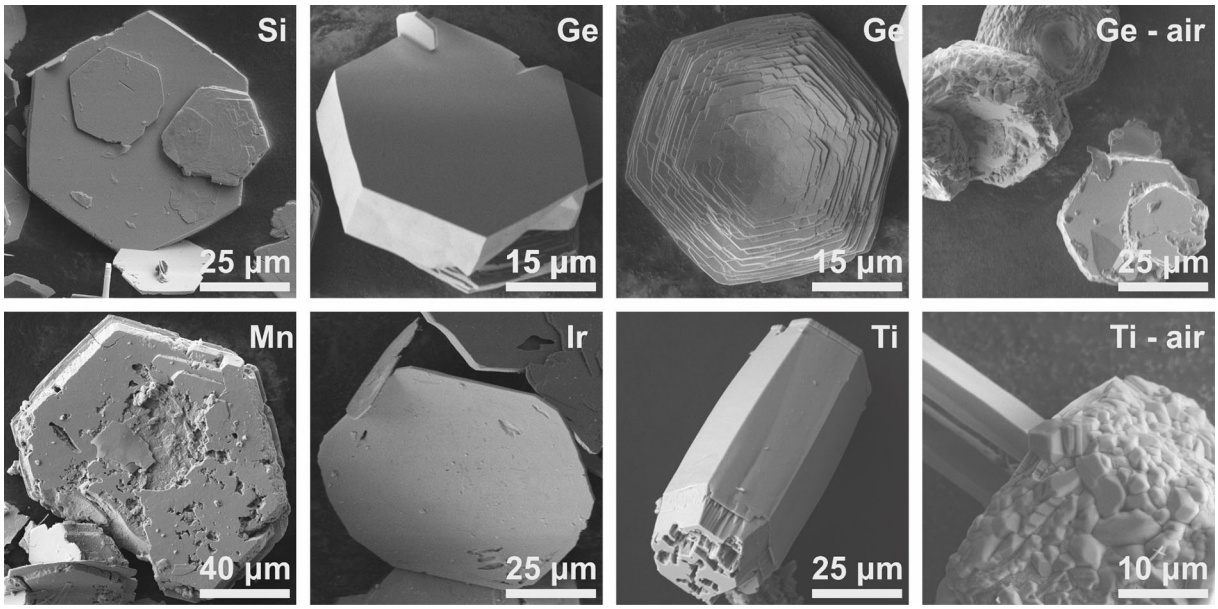

Figure 3. SEM images of typical substituted oxohydroxoferrate $K_{2-x}(Fe,M)_4O_{7-y}(OH)_y$ (M = Si, Ge, Mn, Ir). On the right side, germanium and titanium containing crystals are shown that were exposed to air for over a month.

the hexagonal crystal faces indicate a slight depletion of silicon in the central parts of the crystals (Figure S1, Supporting Information). This might indicate kinetic control of the phase formation, in which silicon is incorporated after an initial crystallization of the oxohydroxoferrate.

Samples of $K_{2-x}(Fe,\mathbf{Ge})_4O_{7-y}(OH)_y$ contained two differently shaped types of crystals, some with smooth surfaces and others with curved, flower-like habit, Figure 3. The latter had a higher germanium content. However, the germanium content found in EDX measurements differs significantly form the ones received by the ICP-OES method. As the latter one is a bulk method and the EDX predominantly gives information about the surface composition, $K_{2-x}(Fe,\mathbf{Ge})_4O_{7-y}(OH)_y$ seems to forms gradient crystals. Similar to the silicon substitution, the ratio of germanium to iron in the product was considerably lower than in the synthesis.

$K_{2-x}(Fe,\mathbf{Ti})_4O_{7-y}(OH)_y$ formed crystal with a hexagonal prismatic shape, which are elongated in z direction. Some crystals had a needle like morphology, others were more compact, but showed rough surfaces. The titanium content in the product nearly matches the starting amount. A small excess of a dissolved titanium species would be removed after the synthesis by the washing process.

Crystals of $K_{2-x}(Fe,\mathbf{Mn})_4O_{7-y}(OH)_y$ exhibited a manifold of morphologies, some with rough surfaces, but all with hexagonal appearance. EDX measurements on several crystals revealed a variable composition, where three kinds of crystals were found: Thin crystals of $K_{2-x}(Fe,\mathbf{Mn})_4O_{7-y}(OH)_y$ with smooth surfaces had the highest manganese and lowest potassium content of all substitutions. Most of the manganese of the starting materials is incorporated in the crystals. The excess of manganese containing compounds seems to be removed by the washing process, as no hints for manganese oxides are found in X-ray powder diffractograms or magnetic measurements (see below).

$K_{2-x}(Fe,\mathbf{Ir})_4O_{7-y}(OH)_y$ exhibits crystal shapes similar to those of the silicon substitution. The Ir-substituted crystals, however, tend to be thinner with more rounded corners of the hexagonal plates. The iridium content of the crystals complies with the starting composition within standard derivations. This seems to be the maximum content, as experiments with more than 7% of iridium indicated.

The analysis of the hydrogen content and thus the charge balancing of the potassium deficit was discussed in detail for the unsubstituted oxohydroxoferrate,[1] where neither NMR-, nor IR-spectroscopy or thermogravimetry (TG) provided significant evidence for hydrogen incorporation. The presence of hydrogen was finally confirmed by carrier gas hot extraction (CGHE) and the quantity was calculated from the potassium deficit by assuming all iron to be in the oxidation state III as confirmed by Mößbauer spectroscopy. For the substituted oxohydroxoferrates, we also performed CGHE to determine the hydrogen content (Table 1). Except for the iridium substituted sample, the results are rather similar to the unsubstituted oxyhydroxoferrate(III), namely about 0.13(1) wt.–% hydrogen.[1] The significantly higher hydrogen content of the iridium sample is well in agreement with the high value for $\Delta_C(x–M)$ of 0.42, which describes the "missing" positive charge resulting from the potassium deficit x diminished by the additional positive charge of the substituting element in oxidation state IV as compared to iron(III). In fact, iridium(IV) should be preferred in the alkaline aqueous system of the hydroflux. The mechanism of the oxidation of iridium(III) in the starting material to iridium (IV) is well known, and no hints for a further oxidation were observed in similar systems to the best of our knowledge.[10]

Moreover, reactions in iron-free systems under similar conditions resulted in hydroxoiridates(IV), too.[11]

For the other substitutions, the charge differences $\Delta_C(x–M)$ are close to zero. Consequently, the potassium deficit should mainly be compensated by the substituting element *M*, which results in a smaller hydrogen content as compared to unsubstituted oxohydroxoferrate if the substituting element is in the oxidation state IV. Besides iridium, this clearly applies to silicon and germanium, and also the reduction of titanium(IV) to titanium(III) is unlikely to occur in a hydroflux. Manganese, however, could exists in oxidation states between II and IV, with higher oxidation states being preferred in basic media.

Overall, the elemental composition of the oxohydroxoferrates is variable with respect to the potassium deficit, the content of hydrogen, and the degree of substitution. Although charge balance must apply, this system includes at least two independent variables. We thus combined information from chemical analyses and crystal structure refinements to determine the compositions of the $K_{2-x}(Fe,M)_4O_{7-y}(OH)_y$ compounds.

Crystal structures and substitution behavior

X-ray diffraction on single-crystals of $K_{2-x}(Fe,M)_4O_{7-y}(OH)_y$ with *M* = Si, Ge, Mn, Ir revealed trigonal structures in the space group $P\bar{3}1\,m$ (no. 162), isostructural to the unsubstituted ferrate (Figure 1, Table 2). In contrast, $K_{2-x}(Fe,\mathbf{Ti})_4O_{7-y}(OH)_y$ crystallizes in the hexagonal space group in $P6_3/mcm$ (no. 193), representing a second polytype with eclipsed tetrahedra in the pillars and doubled *c* axis (Figure S2, Supporting Information). The existence of two polymorphs was already observed for $K_{2-x}Fe_4O_{7-x}(OH)_x$.[1] The oriented intergrowth of domains of the two polytypes can be described by order-disorder (OD) theory.[5,12]

In the structures of $K_{2-x}(Fe,M)_4O_{7-y}(OH)_y$, the substitution can take place on tetrahedral, on octahedral, or on both iron sites simultaneously. For the following discussion of the results of single-crystal X-ray diffraction (SCXRD) experiments, Table 3 provides a compilation of selected bond lengths, angles and ionic radii. The smallest substituting element, *M* = Si, was refined solely on the tetrahedral position, as a lower than expected electron density was found for the iron position Fe2 only. This is reasonable as the tetrahedral coordination is common for silicon in oxidic compounds. The freely refined silicon and potassium contents are well in agreement with the EDX results. Assuming iron(III) and silicon(IV), the sum formula of the investigated crystal is $K_{1.7(1)}\,Fe_{3.8(1)}Si_{0.2(1)}O_{6.9(1)}(OH)_{0.1(1)}$.

Similar to the refinement of the silicon compound, the substituted germanium in $K_{2-x}(Fe,\mathbf{Ge})_4O_{7-y}(OH)_y$ was refined on the tetrahedral position, as a higher electron density was found on the position Fe2. Moreover, residual electron density maxima were found and interpreted as additional oxygen positions, indicating the presence of a minor amount of the hexagonal polytype, see above. Similarly, additional oxygen positions were found in Rietveld refinements against neutron powder data (see below). In the single-crystal data refinements, the second polytype was modelled by introducing a twin domain with twin law (010, 100, 00–1); its volume was refined to 0.7(1) %. Assuming iron(III) and germanium(IV), the sum formula of the investigated crystal is $K_{1.6(1)}\,Fe_{3.7(1)}Ge_{0.3(1)}O_{6.9(1)}(OH)_{0.1(1)}$.

The refinement of the SCXRD data of a red needle-shaped single-crystal of $K_{2-x}(Fe,\mathbf{Ti})_4O_{7-y}(OH)_y$ showed reduced scattering power on both *M* position corresponding to titanium occupancies of 15(1) % on the tetrahedral site and 9(1) % on the octahedral site. Residual electron density was found on the corners of the unit cell, i.e. in the unoccupied octahedral void of the honeycomb net. If this position is occupied, the two adjacent tetrahedral iron positions Fe2 (4*e*, 3.*m*) have to be unoccupied, as the cation distances would be too short (Figure S3, Supporting Information). The refined occupancy of the additional iron position Fe3 (2*b*, $\bar{3}$.*m*) was 3.2(2) %. The

Table 2. Single-crystal structure data of potassium oxohydroxoferrates $K_{2-x}(Fe,M)_4O_{7-y}(OH)_y$ (*M* = Si, Ge, Ti, Mn, Ir) in comparison with the unsubstituted structure.[1]

$K_{2-x}(Fe,M)_4O_{7-y}(OH)_y$	unsubstituted	Si	Ge	Ti	Mn	Ir
x	0.31(3)	0.35(2)	0.41(1)	0.47(1)	0.68(2)	0.66(2)
Refined *M* content per formula unit	–	0.21(1)	0.14(1)	0.48(2)	[a]	0.27(1)
Crystal system	trigonal	trigonal	trigonal	hexagonal	trigonal	trigonal
Space group (no.)	$P\bar{3}1m$ (162)	$P\bar{3}1m$ (162)	$P\bar{3}1m$ (162)	$P6_3/mcm$ (193)	$P\bar{3}1m$ (162)	$P\bar{3}1m$ (162)
Temperature/K	100(1)	100(1)	100(1)	100(1)	100(1)	100(1)
Lattice parameters/pm	a = 517.51(1) c = 692.27(2)	a = 516.72(3) c = 690.39(4)	a = 515.40(1) c = 692.80(2)	a = 515.68(6) c = 1387.2(2)	a = 512.49(1) c = 697.61(2)	a = 515.41(1) c = 699.26(2)
Volume/(10^6 pm^3)	160.56(1)	159.64(2)	159.38(1)	319.47(9)	158.68(1)	160.87(1)
Density (calc.)/(g cm^{-3})	4.152	4.099	4.167	4.121	3.999	4.230
$2\theta_{max}$/°	80	90	90	90	80	90
No. of independent reflections	368	502	514	514	381	517
No. of parameters	23	24	23	28	23	25
R_{int}, R_σ	0.028, 0.011	0.029, 0.012	0.032, 0.012	0.032, 0.010	0.021, 0.006	0.045, 0.022
$R_1[F_o > 2\sigma(F_o)]$, $wR_2(F_o^2)$	0.012, 0.032	0.012, 0.028	0.014, 0.025	0.015, 0.034	0.027, 0.064	0.032, 0.073
GooF(F^2)	1.135	1.190	1.152	1.088	1.113	1.219
Residual electron density/(e 10^{-6} pm^{-3})	+0.71 to −0.68	+0.64 to −0.38	+0.52 to −0.79	+1.15 to −0.49	+2.51 to −1.57	+1.89 to −1.97
Deposition number	CSD-1875190	CSD-2026748	CSD-2026745	CSD-2026746	CSD-2026749	CSD-2026747

[a] Not refined due to similar scattering factors.

Table 3. Selected interatomic distances and angles in the crystal structures of $K_{2-x}(Fe,M)_4O_{7-y}(OH)_y$ (M = Si, Ge, Ti, Mn, Ir) in comparison with the unsubstituted compound.[1] The Fe2–O2–Fe2 angle is 180° by symmetry. Additionally, relevant ionic radii for the substituted elements are provided assuming the oxidation state + IV, whereas the values for iron refer to the oxidation state + III.[13]

M	Fe	Si	Ge	Ti	Mn	Ir
tetrahedral ionic radius/pm	49	26	39	42	39	–
octahedral ionic radius/pm		–	53	60.5	53	68
Fe1–O1/pm	202.4(1)	202.4(1)	202.4(1)	201.0(1)	200.1(1)	201.5(1)
Fe2–O1/pm	187.8(1)	186.9(1)	185.7(1)	187.9(1)	187.6(2)	188.0(1)
Fe2–O2/pm	184.3(1)	184.0(1)	183.9(1)	183.9(1)	183.0(1)	182.9(1)
*M*3–O1/pm	–	–	–	211.8(1)	210.6(2)	211.4(2)
Fe1···Fe1/pm	298.8(1)	298.3(1)	297.6(1)	297.7(1)	295.9(1)	297.6(1)
Fe1···Fe2/pm	339.8(1)	339.1(1)	339.0(1)	339.4(1)	339.2(1)	341.1(1)
Fe2···Fe2[a]/pm	323.6(1)	322.5(1)	325.0(1)	325.9(1)	331.6(1)	333.5(1)
O1–Fe1–O1/°	175.7(1)	176.0(1)	176.6(1)	175.7(1)	175.8(1)	176.1(1)
Fe1–O1–Fe2/°	121.1(1)	121.1(1)	121.7(1)	121.5(1)	122.0(1)	122.2(1)
K(a)–O/pm	288.1(1) – 298.8(1)	287.3(1) – 298.3(2)	–	–	–	–
K(b)–O/pm	268.8(5) – 340.6(8)	266.0(2) – 345.1(6)	274.3(1) – 327.4(1)	275.7(1) – 327.4(1)	278.0(2) - 323.1(3)	278.1(2) – 326.1(3)

[a] Distance across the void in the honeycomb net.

stoichiometric coefficient of (Fe,*M*) in the sum formula, which was four in all previous cases, is here reduced by the occupancy of the Fe3 position. Because this value is small, it does not affect the formula within the given accuracy. Assuming iron(III) and titanium(IV), the sum formula of the investigated crystal is $K_{1.5(1)}Fe_{3.5(1)}Ti_{0.5(1)}O_{7.0(1)}(OH)_{0.0(1)}$. The refined occupancy of the potassium position matches the EDX results.

The refinement of the manganese content in $K_{2-x}(Fe,\mathbf{Mn})_4O_{7-y}(OH)_y$ was not possible based on X-ray data, as iron and manganese have very similar scattering factors. In contrast, neutron diffraction data (see below) left no doubt that manganese is solely found on the octahedral position. The freely refined potassium occupancy results in a deficit of $x = 0.68(1)$. As the manganese content is very similar to x, manganese in oxidation state IV can be assumed. Analogous to the titanium compound, the Fe3 position is occupied by 8.0(4) %. With iron(III) and manganese(IV), the sum formula of the investigated crystal is $K_{1.3(1)}Fe_{3.2(1)}Mn_{0.7(1)}O_{7.0(1)}(OH)_{0.0(1)}$.

The SCXRD refinement of $K_{2-x}(Fe,\mathbf{Ir})_4O_{7-y}(OH)_y$ showed additional electron density on the octahedral position only. This matches the expectations as iridium(IV) is very unlikely to adopt a tetrahedral oxygen coordination. However, the refined iridium content on Fe1 is lower than the total iridium content derived from EDX measurements. Similar to the structure of titanium and manganese substituted samples, additional electron density was found on the corners of the unit cell. As iridium(IV) has a larger ionic radius than iron(III) and the empty octahedral void in the honeycomb is about 5% larger, the additional position (*M*3) is most likely occupied by iridium. With this slightly adjusted model, the overall iridium content in the structure matches the EDX results with a substitution rate of iridium of 12.0(2) % on Fe1 and an occupancy of 2.5(2) % on the Ir3 site. The freely refined potassium content fits to the EDX results within standard deviations. Assuming iron(III) and iridium(IV), the sum formula of the investigated crystal is $K_{1.3(1)}Fe_{3.7(1)}Ir_{0.3(1)}O_{6.6(1)}(OH)_{0.4(1)}$.

Potassium ordering

The potassium atoms of each structure are coordinated by nine oxygen atoms, which form a distorted tri-capped trigonal antiprism. Neighboring coordination polyhedra share a rectangular face of about 300×400 pm^2 (diagonals about 500 pm). Literature data for the effective diameters of potassium and oxide ions are 260–300 pm and 260–280 pm, respectively. Taking the inadequacies of a static hard sphere model into account, the passage of a potassium cation through such a face appears to be possible but probably hindered.

The oxohydroxoferrates can be divided in three groups according to their potassium deficit obtained by the ICP-OES measurements (see above). In case of the unsubstituted ferrate as well as for M = Si, a potassium deficit of $x \approx 1/3$ is found. These two compounds are the only ones that have two partially occupied positions: K(a) (Wyckoff position 2*d*, site symmetry 3.2) and K(b) (6*j*, ..2; Ti: 12*j*, *m*..), see Figure 1. Modelling the potassium ordering for $x \approx 1/3$ leads to a tripling of the *a* and *b* axes (Figure 4). In this superstructure, 18 potassium positions are included, where six potassium atoms are found on the K(a) position and nine potassium atoms are located on the K(b) positions with an elongated ellipsoid pointing towards the three vacant potassium positions.

The next group with a potassium deficit of $x \approx 1/2$ includes the germanium and titanium substitutions. Here only K(b) is occupied with an occupancy of 0.25. This corresponds with our previously discussed $2a \times 2b$ superstructure model for a hypothetical compound $K_{1.5}Fe_4O_{6.5}(OH)_{0.5}$ (i.e. $x = 0.5$),[1] which is now realized (Figure 4).

The third group with a potassium deficit of $x \approx 2/3$ comprises the manganese and iridium substitutions. The potassium order can again be described in a $3a \times 3b$ superstructure, in which one of three potassium positions is vacant and the distance between these voids is maximized (Figure 4). In this model, one quarter of the potassium atoms has three potassium neighbors, while the remaining three quarter have only one neighbor.

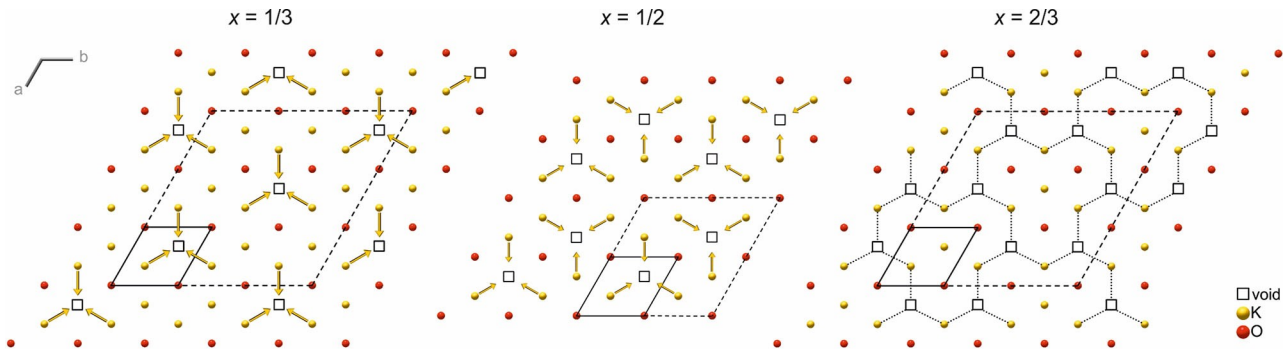

Figure 4. Superstructure models of $K_{2-x}(Fe,M)_4O_{7-y}(OH)_y$ for potassium deficits of $x = 1/3$ (left), $x = 1/2$ (middle) and $x = 2/3$ (right) with an enlarged unit cells (dashed lines) assuming an ordering of voids and potassium positions. The arrows indicate the direction of the shift of the potassium atoms towards the adjacent voids.

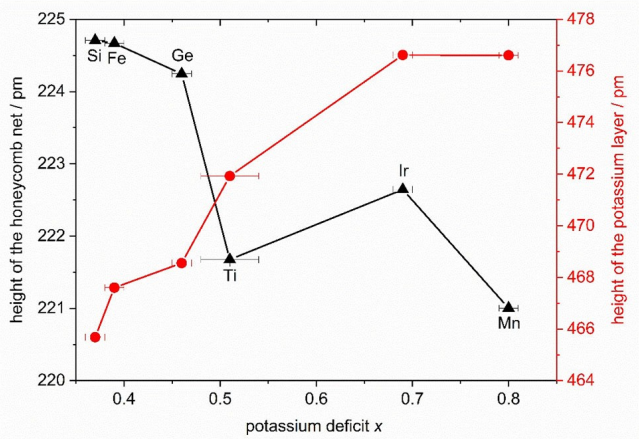

Figure 5. Heights of the honeycomb net (black) and the potassium layer (red) in $K_{2-x}(Fe,M)_4O_{7-y}(OH)_y$ (M = Si, Ge, Ti, Mn, Ir) in relation to the potassium deficit x. The standard derivations of the metrical parameters are much smaller than the symbols.

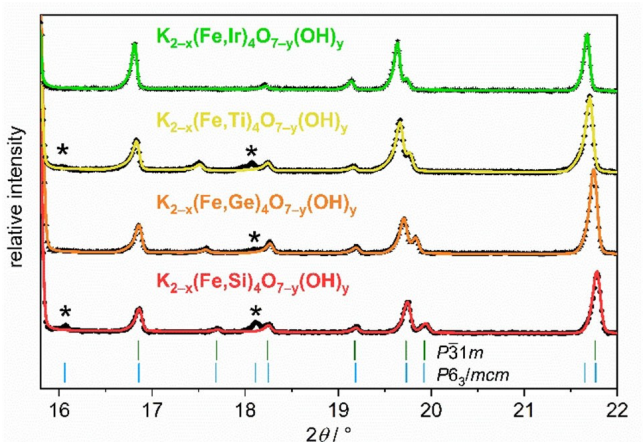

Figure 6. PXRD patterns of $K_{2-x}(Fe,M)_4O_{7-y}(OH)_y$ (M = Si, Ge, Ti, Ir). Additional reflections of the hexagonal polytype are marked with an asterisk.

Structural details

The structure of the substituted oxohydroxoferrates is influenced by several factors, where the ionic radius of the substituted element, its content and the potassium deficit are decisive ones. With a closer look on the lattice parameters, all substitutions except for silicon have a longer c axis. This lattice parameter is the sum of the heights of the potassium layer and the honeycomb net (Figure S4, Supporting Information). Both are roughly correlated with the potassium deficit x (Figure 5): the larger x the thicker the potassium layer. The reduced electrostatic attraction between potassium and oxygen atoms might be the cause. The potassium content also influences the length of the Fe2–O2 bonds, as fewer potassium atoms are coordinated to O2 result in stronger Fe2–O2 bonds.

Notably thinner honeycomb nets were found for substitutions replacing Fe1 (M = Ti, Ir, Mn). In these cases, many influences combine: charge and content of M, partial filling of the $M3$ position and depopulation of the Fe2 position as well as the potassium deficit x. Remarkably the a (and b) axes of all substituted samples are smaller than for the unsubstituted one.

Rietveld refinements of powder X-ray diffraction data

Rietveld refinements against PXRD data of the substituted oxohydroxoferrates were performed to gain information about purity and homogeneity of the samples and, if possible, the bulk composition with respect to the potassium deficit and the degree of substitution (Table S1 and Figure S5 to Figure S9, Supporting Information). For each substituted oxohydroxoferrate, residual electron density maxima were found on the same positions as already described in the SCXRD data. Twinning with sufficiently large domains does not affect powder diffraction data, so that the residual electron density can be attributed to an alternative stacking sequence, i.e. the $P6_3/mcm$ polytype. Additional reflections that double the c-axis in this space group were most intensive in the powder patterns of M = Ti or Si (Figure 6, Figure S10 and Figure S11). In contrast to the result of the SCXRD analysis, the Rietveld refinement showed that the titanium substituted compound also adopts both polytypes. Overall, the

Table 4. Structure refinement data from neutron diffraction experiments on $K_{2-x}(Fe,M)_4O_{7-y}(OH)_y$ (M = Si, Ge, Ti, Ir). All structures were refined in the trigonal space group $P\bar{3}1c$ (no. 163). The results for $K_{2-x}(Fe,\mathbf{Mn})_4O_{7-y}(OH)_y$ are poor due to broad and asymmetrical reflections caused by the different phases in this sample, see text for details.

$K_{2-x}(Fe,M)_4O_{7-y}(OH)_y$	Si		Ge		Ti		Ir	
Wavelength/pm	154.83		159.4		154.83		159.4	
Temperature/K	4	300	5	295	4	300	5	295
a/pm	515.169(3)	515.910(4)	514.633(3)	515.313(3)	515.285(3)	515.918(3)	516.188(2)	516.90(2)
c/pm	1379.16(2)	1380.83(2)	1389.30(2)	1390.61(2)	1388.35(2)	1389.98(2)	1396.58(2)	1398.30(2)
Volume/ (10^6 pm^3)	316.99(1)	318.28(1)	318.66(4)	319.80(1)	319.25(1)	320.41(1)	322.26(1)	323.55(1)
Density (calc.)/(g cm^{-3})	4.13(1)	4.11(1)	4.13(1)	4.12(1)	4.07(1)	4.05(1)	4.38(1)	4.34(1)
$2\theta_{max}$/°	156	156	160	160	156	156	147	160
No. of parameters	14	14	14	14	14	14	14	14
R_p, wR_p	0.026, 0.036	0.030, 0.040	0.043, 0.043	0.036, 0.035	0.037, 0.046	0.037, 0.046	0.043, 0.041	0.044, 0.039
gof	2.06	1.93	1.86	1.68	2.81	2.56	1.84	1.66
Resid. electron dens./ (e 10^{-6} pm^{-3})	−0.67 – +0.83	−0.83 – +0.78	−1.05 – +0.96	−0.59 – +0.79	−0.95 – +0.84	−0.99 – +0.77	−1.40 – +0.97	−0.88 – +1.02
$m_{z,Fe1}$ (Fe1/*M*1)	4.24(5)	4.08(6)	4.63(3)	4.21(3)	4.31(7)	3.87(7)	4.22(8)	4.04(7)
$m_{z,Fe2}$ (Fe2)	−3.83(5)	−3.49(5)	−3.26(3)	−2.96(3)	−3.92(5)	−3.75(5)	−3.91(6)	−3.63(6)
$\Delta(m_{z,Fe1}-m_{z,Fe2})$	0.41(5)	0.59(6)	1.37(3)	1.25(3)	0.39(7)	0.12(7)	0.31(8)	0.41(7)

refined content of the respective substituted element *M* and the potassium deficit were found to be in good agreement with the ICP-OES, EDX, and SCXRD results. The powder diffraction pattern of $K_{2-x}(Fe,\mathbf{Mn})_4O_{7-y}(OH)_y$ showed broad and asymmetrical reflections, probably due to different degrees of substitution (as revealed by EDX). The homogeneity range is associated with a slight variation of the lattice parameter.

Rietveld refinements of neutron powder diffraction data

Two neutron powder diffractograms were measured for each substituted oxohydroxoferrate, one near room temperature and one at 4 K (samples measured at SPODI/FRM II, Garching) or 5 K (samples measured at D2B/ILL, Grenoble). Detailed information can be found in Table 4. The diffraction patterns at the two temperatures are nearly identical in each case (Figure S12, Supporting Information), suggesting magnetic ordering Néel temperatures (T_N) above room temperature. T_N of the unsubstituted ferrate is at least 800 K.[1] In addition, the diffraction patterns of all substituted phases resemble each other in positions and intensities of their reflections (Figure 7). The pattern of $K_{2-x}(Fe,\mathbf{Mn})_4O_{7-y}(OH)_y$ is slightly different with respect to broadness and asymmetric shape of the reflections, as had been observed in the PXRD measurements. Due to the assumed presence of a mixture with different degrees of substitution in this case, the results of the refinement are not discussed in detail.

All neutron diffraction patterns had a relatively low background and a good signal to noise ratio, which is unusual for hydrogen containing compounds. The relatively low hydrogen content, but also the large coherent scattering cross section of iron[14] and the high crystallinity of the products from hydroflux syntheses might be reasons for that. Nonetheless, the positions

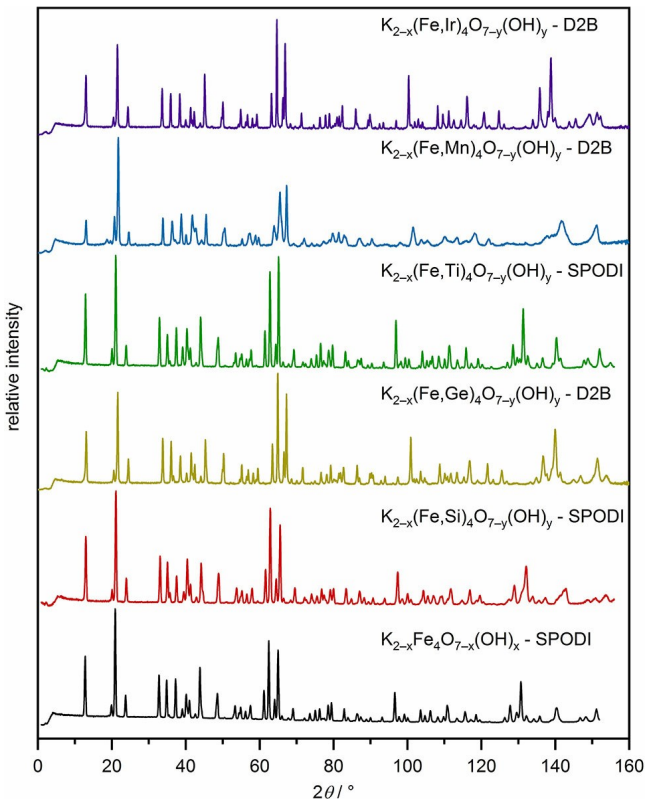

Figure 7. Neutron diffraction patterns of $K_{2-x}(Fe,M)_4O_{7-y}(OH)_y$ (M = Si, Ge, Ti, Mn, Ir) in comparison with the unsubstituted compound.[1] The measurement temperature was 4 or 5 K. Note the slightly different wavelengths (see Table 4).

of the hydrogen atoms could not be located from the scattering data, probably due to disorder.

The magnetic scattering contributions indicate a magnetic propagation vector of $k = (0, 0, {}^1/_2)$ for all substituted oxohy-

droxoferrates (Figures S13–S21, Supporting Information). Following the group-subgroup formalism for the nuclear structure, the doubling of the *c* axis of the trigonal polytype corresponds to a *klassengleich* transition of index 2 from $P\bar{3}1m$ to $P\bar{3}1c$ (no. 163). The symmetry analysis for the magnetic data indicated four possible Shubnikov groups compatible with the propagation vector.[15,16] A reasonable fit, however, was only obtained in space group $P\bar{3}1c$ (no. 163.1.1310)[16] for all compositions (Figures S14 to S21, Supporting Information). Even in case of $K_{2-x}(Fe,\mathbf{Ti})_4O_{7-y}(OH)_y$, a fitting of the magnetic scattering intensities in Shubnikov groups with hexagonal symmetry failed or gave unsatisfying *R*-values, so that group $P\bar{3}1c$ was considered for this compound, too.

The enlargement of the (magnetic) unit cell generated two crystallographic inequivalent potassium positions, K1 (2*d*, 3.2; 2/3, 1/3, 1/4) and K2 (2*c*, 3.2; 1/3, 2/3, 1/4). Both potassium positions were refined with the same occupancy. Another difference between the space groups $P\bar{3}1c$ and $P\bar{3}1m$ is the free *z* parameter of the octahedral iron position Fe1. Small derivations from zero were observed during the structure refinement of the titanium and germanium substituted samples. A corrugation of the honeycomb net appears plausible if the potassium atoms order along the *c* direction. This effect is clearly discernible in the structure of $BaFe_4O_7$, where every second position in the cavity between the ferrate layers is unoccupied.[4] However, the nuclear structure of the barium compound was refined in $P\bar{3}1c$ with a doubled *c* axis. As for $K_{2-x}(Fe,M)_4O_{7-y}(OH)_y$ (*M* = Si, Ge, Ti, Mn, Ir) no additional reflection were visible in the diffraction pattern of the SCXRD experiments, the *z* parameter of the Fe1 positions was set to zero.

For the titanium and silicon substituted ferrates, the parallel refinement of the trigonal and hexagonal polymorph against the neutron diffraction data resulted in similar polymorph ratios as found for the PXRD data. For $K_{2-x}(Fe,\mathbf{Ir})_4O_{7-y}(OH)_y$, residual electron density was found in the voids of the honeycomb nets similar to the SCXRD refinement. The refinement of both phenomena lead to a better fit of the diffraction pattern, however, also introducing new correlations. To avoid additional parameters and to obtain accurate values for the magnetic moments of the Fe1 and Fe2 position, all compositions were fixed to the values of the ICP-OES analyses.

For all substituted compounds, the magnetic vectors nearly cancel each other out, similar to those of $K_{2-x}Fe_4O_{7-x}(OH)_x$ ($m_{z,Fe1}$ = 4.18(4) μ_B, $m_{z,Fe2}$ = 3.97(4) μ_B at 4 K).[1]. Both magnetic moments are significantly reduced as compared to the spin-only value of 5 μ_B for iron(III). Similar deviations had been observed for, e.g., Sr_2FeO_3F or $Y_3Fe_5O_{12}$ and might be attributed to a covalent contribution to the Fe–O bonds.[17,18] Upon lifting the symmetry restrictions for the individual moments of Fe1 and Fe2, no significant contributions along the *a* and *b* directions were computed, in contrast to the magnetic structure of $BaFe_4O_7$.[4]

Magnetic properties

The magnetic structure of the substituted oxohydroxoferrates resembles the unsubstituted compound (Figure 8). The spins of the iron atoms within the octahedral layer (Fe1) order ferromagnetic, while the iron atoms in the tetrahedra (Fe2) are coupled antiferromagnetic to all adjacent Fe2 and Fe1 atoms. This spin arrangement can be explained by the Goodenough-Kanamori-Anderson rules,[19–21] which postulate ferromagnetic coupling between (octahedral coordinated) iron atoms if the Fe1–O1–Fe1 angle is close to 90° and antiferromagnetic interaction for angles close to 180°. Moreover, the linear Fe2–O2–Fe2 angle in the oxohydroferrates should give rise to a strong antiferromagnetic superexchange coupling. The antiferromagnetic spin alignment in the iron tetrahedra leads to an opposite orientation of the spins in adjacent octahedral layers. Overall, all spins of iron atoms with the same *z* parameter point in the same direction.

The magnetic susceptibilities $\chi(T)$ of the oxohydroxoferrates were measured between 1.8 and 300 K in a field of 100 mT. In the whole temperature range, no signs of a magnetic transition (e.g. hinting for a weak ferromagnetism from spin canting) were found in the temperature-depended measurements, which is in accordance with the neutron diffraction experiments. However, in every sample a small ferromagnetic impurity was detected, which had not been visible in the diffraction experiments. As ferromagnets saturate at high fields, measurements were performed at various temperatures with fields up to 9 T. The magnetic susceptibilities χ_{mol} was determined from the linear part of the curve in the *M*-*H* plot at fields above 5 T. The thereof derived magnetic susceptibility of the oxohydroferrates is small, paramagnetic and largely temperature independent (Figure 9), in accordance with the long-

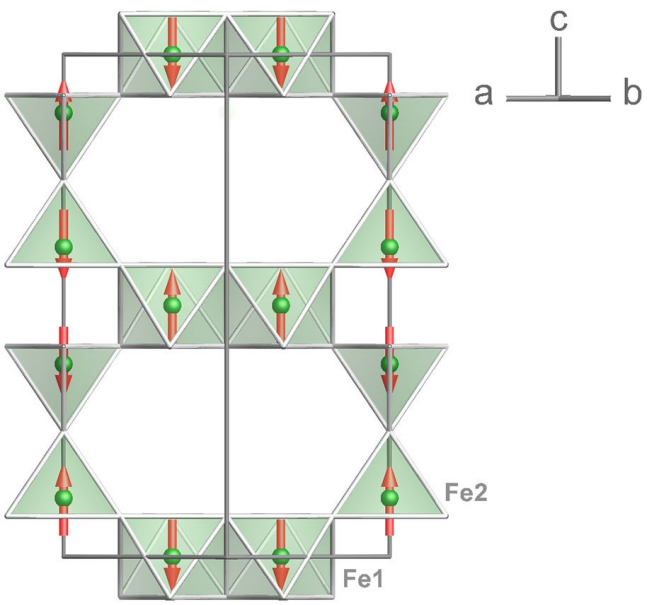

Figure 8. Antiferromagnetic order in $K_{2-x}(Fe,M)_4O_{7-y}(OH)_y$ (*M* = Si, Ge, Ti, Mn, Ir). The refined magnetic moments are listed in Table 4.

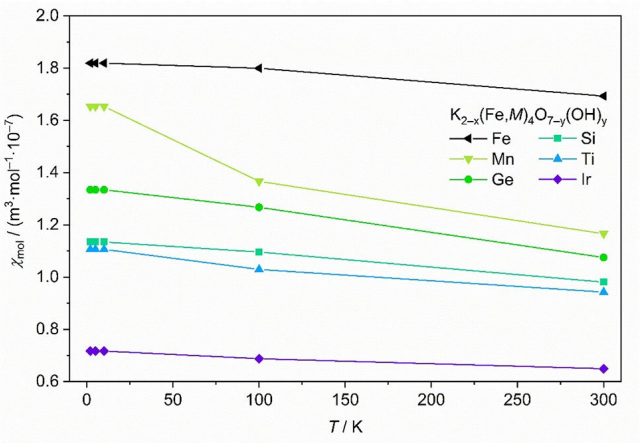

Figure 9. Magnetic susceptibility of $K_{2-x}(Fe,M)_4O_{7-y}(OH)_y$ (M = Si, Ge, Ti, Mn, Ir) in comparison with the unsubstituted ferrate.[1]

range antiferromagnetic ordered state at temperatures well below T_N.

Potassium ion conductivity

Crystalline samples of every oxohydroxoferrate were ground to fine powders using a ball mill and then cold pressed into pellets. One pellet of each sample was measured immediately after the preparation, another was annealed in air at 700 °C for 12 h and measured right after. In both cases, the intermediate contact time with air at room temperature was kept short. After contacting with a silver paste, the potassium ion conductivity was analyzed by electrochemical impedance spectroscopy (EIS) in a frequency range between 1 MHz and 100 mHz at ambient temperature. The recorded impedance was visualized in a Nyquist plot demonstrating the expected behavior of an ion conductor, for which a semicircle and a linear part are present (Figure 10 and S22 to S33, Supporting Information). The semicircle arises from the capacitance and ohmic resistance of the sample, while the linear part is a product of the Warburg effect. For some samples, especially for the EIS measurements of $K_{2-x}(Fe,\mathbf{Ti})_4O_{7-y}(OH)_y$, induction effects are also present leading to distorted semicircles. The impedance of the samples was determined, if possible, by a circle fit or, if not, by fitting the linear part. The ion conductivity was calculated by dividing the thickness of the pellet by the impedance and the surface area (Table S2, Supporting Information).

The ionic conductivities of the oxohydroxoferrates are visualized in Figure 11. Overall, an increase of the ion conductivity is visible after the annealing process, where oxohydroxoferrates with a higher potassium deficit tend to have a larger ion conductivity. The largest ion conductivity was found for annealed $K_{1.3(1)}Fe_{3.7(1)}\mathbf{Ir}_{0.3(1)}O_{6.6(1)}(OH)_{0.4(1)}$ with $5.0 \cdot 10^{-3}$ S cm^{-1} and for annealed $K_{1.5(1)}Fe_{3.9(1)}\mathbf{Ge}_{0.1(1)}O_{6.6(1)}(OH)_{0.4(1)}$ with $1.3 \cdot 10^{-3}$ S cm^{-1}. The annealed sample of $K_{1.6(1)}Fe_{3.7(1)}\mathbf{Si}_{0.2(1)}O_{6.8(1)}(OH)_{0.2(1)}$ had an even smaller ion conductivity than the untreated sample, which might be caused by a temperature-induced reaction between the acidic silicate and potassium hydroxide. Similar to the unsubstituted oxohydroxoferrate, $K_{2-x}(Fe,M)_4O_{7-y}(OH)_y$ (M = Si, Ge, Ti, Mn, Ir) do not decompose at 700 °C (Figure S34, Supporting Information).

For unsubstituted $K_{2-x}Fe_4O_{7-x}(OH)_x$ it had been observed that potassium oxide and hydroxide segregate under ambient conditions and heating accelerates this process.[1] As-synthesized samples of $K_{2-x}(Fe,\mathbf{Ge})_4O_{7-y}(OH)_y$ and $K_{2-x}(Fe,\mathbf{Ti})_4O_{7-y}(OH)_y$ showed the same behavior at room temperature, yet apparently slower than the unsubstituted oxohydroxoferrate. Ball-milling drastically increased the surface area and induced faster segregation of potassium hydroxide, also for other M substitutions. After one day in air, a pellet of freshly ground $K_{2-x}(Fe,\mathbf{Ti})_4O_{7-y}(OH)_y$ was covered with an alkaline moisture film (Figure S35, Supporting Information). The loose ball-milled powder got clumpy and sticky after several days in air. Pressing of this aged powder resulted in a very dense and crack-free pellet together with a pressed out yellowish viscous alkaline liquid, probably a highly concentrated and partially carbonated KOH solution (Figure S36, Supporting Information). The wetting of the solid by liquid KOH drastically improved the measured ion conductivity. Aged samples of $K_{2-x}(Fe,M)_4O_{7-y}(OH)_y$ (M = Ge,

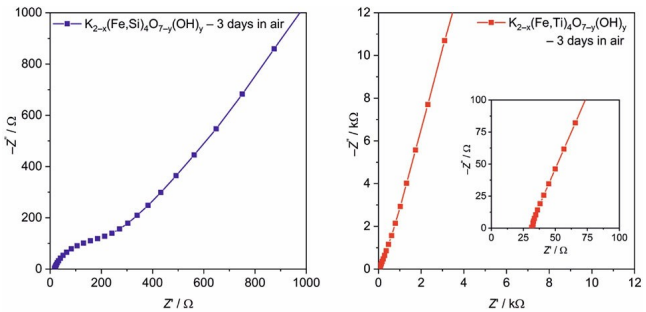

Figure 10. Nyquist plots of impedance measurements recorded at room temperature on cold pressed pellets of aged $K_{2-x}(Fe,\mathbf{Si})_4O_{7-y}(OH)_y$ (left) and $K_{2-x}(Fe,\mathbf{Ti})_4O_{7-y}(OH)_y$ (right).

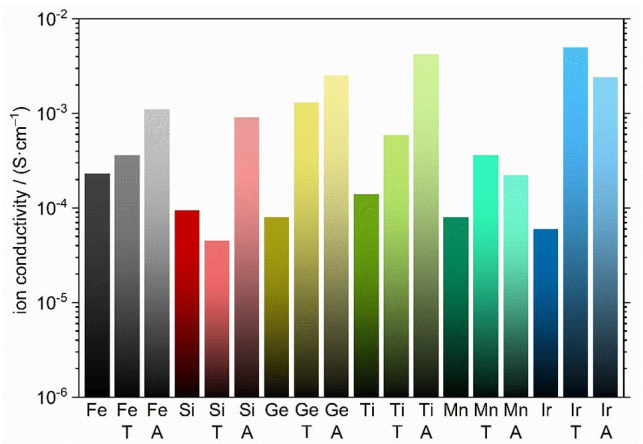

Figure 11. Potassium ion conductivity of ball-milled samples of $K_{2-x}(Fe,M)_4O_{7-y}(OH)_y$ (M = Fe, Si, Ge, Ti, Mn, Ir) measured at room temperature. "T" marks annealed samples and "A" stands for aged samples.

Ti, Ir) had an up to 30 times higher ion conductivity at room temperature than the freshly ground ones. The highest value, $4.2 \cdot 10^{-3}$ S cm^{-1}, was measured for a pellet of aged $K_{2-x}(Fe,\mathbf{Ti})_4O_{7-y}(OH)_y$.

Annealing the aged pellets at 700 °C decreased the ion conductivity to less than 10^{-6} S cm^{-1}. Obviously, the liquid phase on the surface had been dried. Moreover, no impedance could be determined for the samples with M = Mn or Ir. Hydrolysis in air and subsequent annealing had further decreased the already low potassium content so that the structure collapsed.

The ion conductivity depends on the concentration and mobility of the potassium cations, which is of course very high in a liquid KOH phase wetting a compressed powder. In the solid oxohydroxoferrates, the successful hopping transport of potassium atoms necessitates a sufficiently high number of unoccupied K positions. The samples with the lowest potassium content thus show the highest conductivity. The potassium content can be reduced by substitution, partial hydrolysis in air at room temperature, or by annealing. However, the pillar layers in the structure collapse if too much potassium is removed.

The potassium ion conductivity at room temperature of our unsubstituted $K_{2-x}Fe_4O_{7-x}(OH)_x$ ($3.6 \cdot 10^{-4}$ S cm^{-1}) is two orders of magnitude lower than the one reported for "$K_2Fe_4O_7$" ($5.0 \cdot 10^{-2}$ S cm^{-1}), which has basically the same structure and was annealed following a similar procedure.[7] The room temperature ion conductivity in the here presented annealed $K_{2-x}(Fe,Ir)_4O_{7-y}(OH)_y$ ($5.0 \cdot 10^{-3}$ S cm^{-1}) is much higher than in the unsubstituted ferrate and equivalent or even better than in standard sodium or potassium ion conductors, like β-aluminate-type ferrates ($K_{1.3}Fe_{11}O_{17}$, $3.5 \cdot 10^{-3}$ S cm^{-1}),[22,23] β-aluminates (polycrystalline β''-aluminate, $1 \cdot 10^{-3}$ S cm^{-1}),[24] or sodium super ionic conductors (NASICON, $Na_{3.1}Zr_{1.95}Mg_{0.05}Si_2PO_{12}$, $3.5 \cdot 10^{-3}$ S cm^{-1}).[25,26]

Conclusions

Phase-pure samples (8 g) of the substituted oxohydroxoferrates $K_{2-x}(Fe,M)_4O_{7-y}(OH)_y$ (M = Si, Ge, Ti, Mn, Ir) were obtained from hydroflux syntheses using a potassium hydroxide hydroflux with a base-water ratio q(K) of about 0.9. It was found that the composition of the hydroflux medium has to be adapted to the batch size and the autoclave type. In addition, the reaction parameters had to be adjusted for the specific element M to prevent side phases. X-ray and neutron diffraction revealed that all these compounds exist in two polytypes, one crystallizing in the trigonal space group $P\bar{3}1m$ and the other in the hexagonal space group $P6_3/mcm$ with doubled c axis. Typically the trigonal polymorph dominates, but single-crystals of the hexagonal polymorph of $K_{2-x}(Fe,\mathbf{Ti})_4O_{7-y}(OH)_y$ were also found. The achieved degrees of metal substitution vary between 5 and 20%, which basically does not affect the antiferromagnetic long-range order in this type of ferrates. On the other hand, the potassium content could be reduced down to x = 0.8, which increased the ion conductivity substantially. Further improvements of the ion conductivity were achieved by annealing the samples at 700 °C and hydrolysis in air; both procedures cause the segregation of potassium oxide or hydroxide. The highest achieved potassium ion conductivity was $5 \cdot 10^{-3}$ S cm^{-1} (M = Ir). Higher ion conductivity might be caused by partial hydrolysis, which leads to wetting of compressed powders by highly concentrated liquid KOH.

Experimental Section

Synthesis

The substituted oxohydroxoferrates $K_{2-x}(Fe,M)_4O_{7-y}(OH)_y$ (M = Si, Ge, Ti, Mn, Ir) were synthesized in potassium hydroxide hydroflux reactions. Syntheses were carried out in PTFE-lined 250 mL Berghof type HR-200 autoclaves to prevent loss of water. The hydroflux consisted of 160 g potassium hydroxide (86%, Fisher Scientific) and 48 mL deionized water, except 50 mL for the germanium and 55 mL for the titanium substitution. The potassium hydroxide has to be added slowly in 20 g portions to avoid boiling. Additionally, the PTFE inlet was cooled with cold water. Before adding the potassium hydroxide, 29.5 g (73 mmol) of $Fe(NO_3)_3 \cdot 9H_2O$ ($\geq$ 98%, Sigma Aldrich) and the additional starting material (SiO_2: 0.88 g, 14.6 mmol, p.a., Honeywell; GeO_2: 5.23 g, 50 mmol, 99.999%-Ge, abcr; TiO_2: 1.14 g, 14.6 mmol, 99.9%, Alfa Aesar; $Mn(NO_3)_2 \cdot 6H_2O$: 4.19 g, 14.6 mmol, $\geq$ 97%, Sigma Aldrich; $IrCl_3 \cdot 3H_2O$: 2.54 g, 7.2 mmol, 99.9%-Ir, abcr) were dissolved/suspended in the deionized water. In the case of the germanium substitution 20.2 g (50 mmol) of $Fe(NO_3)_3 \cdot 9H_2O$ were added. The autoclave was heated to 200 °C with 2 K min^{-1} and held for 15 h at this temperature before cooling to room temperature at the rate of 0.5 K min^{-1}. The products were washed quickly with deionized water to pH neutrality and once with ethanol to improve the drying process. After the washing, the products were dried in vacuum and stored under argon.

Crystal structure determination

Intensity data was collected at 100(1) K with the four-circle diffractometers Kappa Apex2 (Bruker) for M = Si, Ti, Mn and SuperNova (Rigaku Oxford Diffraction) for M = Ge, Ir equipped with a CCD-detector using graphite-monochromated Mo–Kα radiation (λ = 71.073 pm). The raw data were corrected for background, Lorentz and polarization factors[27], and multi-scan absorption correction was applied.[28] The structures were solved using ShelXT.[29] Structure refinement against F_o^2 with ShelXL[30] included anisotropic displacement parameters for all atoms. Graphical representations of the structure were developed with Diamond.[31] Table 2 and Table S3 to Table S7 of the Supporting Information contains crystal structure data. Further details of the crystal structure determination are available on quoting the depository numbers listed in Table 2.

Deposition Numbers 1875190, 2026748, 2026745, 2026746, 2026749, and 2026747 contain the supplementary crystallographic data for this paper. These data are provided free of charge by the joint Cambridge Crystallographic Data Centre and Fachinformationszentrum Karlsruhe Access Structures service www.ccdc.cam.ac.uk/structures.

Powder X-ray diffraction

Phase identification and purity examinations were performed by PXRD at room temperature on an STADI P diffractometer (Stoe &

Cie.) equipped with a Dectris Mythen 1 K detector using Ge monochromated Mo-$K\alpha_1$ radiation ($\lambda = 70.932$ pm). The program package Topas-Academics v.5 was used for Rietveld refinement.[32]

Neutron powder diffraction

The nuclear and magnetic characterization of $K_{2-x}(Fe,M)_4O_{7-y}(OH)_y$ with M = Si, Ti was carried out on the SPODI high-resolution powder diffractometer at the research reactor Heinz-Maier-Leibnitz (FRM II) in Munich. Diffraction data were collected at 4 K and 300 K using a closed-cycle cryostat and a Ge(551) monochromator with a neutron wavelength of $\lambda = 154.83$ pm and a step width of 0.05°. The detector bank consists of 80 spatially resolved ^{3}He counter tubes (active measuring height: 300 mm; 2° angular range).[33,34] Data for M = Ge, Mn, Ir were measured at the Institute Laue-Langevin (ILL) in Grenoble, using the D2B instrument with a wavelength of $\lambda =$ 159.4 pm and the 10′′ primary collimator at 5 K and 298 K. Diffraction data were collected in 25 steps with a step width of 0.05°.[35] The refinement of the nuclear and magnetic structure was done with Jana2006.[36] To minimize correlations, the components of the magnetic moments that were refined to 0 within 3σ were fixed at this value. Table 4 and Table S8 of the Supporting Information contains crystal structure data.

Impedance spectroscopy

The oxohydroxferrates $K_{2-x}(Fe,M)_4O_{7-y}(OH)_y$ (M = Fe, Si, Ge, Ti, Mn, Ir) were ground using a planetary ball-mill and pressed into pellets with a diameter of 10 mm and a thickness of about 1 mm. Of each kind, one pellet was measured immediately and another was annealed in air at 700 °C for 12 h. Silver paste was used for contacting. The ion conductivity was measured with the AC impedance method using a VMP-3 (Biologic) potentiostat. The data were collected in the range between 1 Hz and 1 MHz with an applied AC voltage of 10 mV.

Magnetic measurements

The magnetic properties were analyzed with a CRYOGENIC Cryogen Free Measurement System (CFMS). The measured data were recorded using a Vibration Sample Magnetometer (VSM) in the temperature range from 1.8 K to 300 K. The compound $K_{2-x}(Fe,\mathbf{Ti})_4O_{7-y}(OH)_y$ was analyzed with a SQUID magnetometer MPMS3 from Quantum Design in VSM mode in the temperature range from 1.8 K to 300 K.

SEM and EDX analysis

Scanning electron microscopy (SEM) was performed using a SU8020 (Hitachi) with a triple detector system for secondary and low-energy backscattered electrons ($U_a = 5$ kV). The composition of selected single crystals was determined by semi-quantitative energy dispersive X-ray analysis ($U_a = 15$ kV) using a Silicon Drift Detector (SDD) X–Max^N (Oxford Instruments). The data were processed (integration, pulse-pile up correction) applying the AZtec software package (Oxford Instruments, 2013).

ICP-OES

The ICP-OES measurements were carried out on an Optima 7000 DV optical emission spectrometer (Perkin-Elmer) that can process the wavelength range of 160–900 nm with a high-resolution echelle optics (30° CaF_2 prism) on an SCD detector (resolution < 7 pm).

Carrier gas hot extraction

The hydrogen content of $K_{2-x}(Fe,M)_4O_{7-y}(OH)_y$ (M = Si, Ge, Ti, Mn, Ir) was analyzed with a TCH600 carrier gas hot extraction system from Leco.

Acknowledgements

We thank Prof. Dr. K. Merzweiler and *Prof. Dr. S. Ebbinghaus* (Martin-Luther-Universität Halle-Wittenberg) for the opportunity to use their IR-spectrometer and PXRD device. We are thankful to *Prof. Dr. J. J. Weigand*, TU Dresden, for SCXRD measurements. We are indebted to *U. Schmidt* and *Dr. G. Auffermann* (Max-Planck-Institut für Chemische Physik fester Stoffe, Dresden) for chemical analyses. This work was financially supported by the Deutsche Forschungsgemeinschaft (DFG) within the SFB 1143 "Correlated Magnetism – From Frustration to Topology", project-id 247310070 (Project B03). Open access funding enabled and organized by Projekt DEAL.

Conflict of Interest

The authors declare no conflict of interest.

Keywords: Ion conductivity · Ferrate · Crystal structure · Magnetic structure · Hydroflux synthesis

[1] R. Albrecht, J. Hunger, T. Block, R. Pöttgen, A. Senyshyn, T. Doert, M. Ruck, *ChemistryOpen* **2019**, *8*, 74–83.
[2] D. E. Bugaris, M. D. Smith, H.-C. zur Loye, *Inorg. Chem.* **2013**, *52*, 3836–3844.
[3] R. Albrecht, J. Hunger, M. Hölzel, T. Block, R. Pöttgen, T. Doert, M. Ruck, *ChemistryOpen* **2019**, *8*, 1399–1406.
[4] T. Ferreira, G. Morrison, W. M. Chance, S. Calder, M. D. Smith, H.-C. zur Loye, *Chem. Mater.* **2017**, *29*, 2689–2693.
[5] T. Matsuzaki, K. Hagiya, A. Shatskiy, T. Katsura, M. Matsui, *J. Mineral. Petrol. Sci.* **2010**, *105*, 303–308.
[6] H. Yang, J. Konzett, C. T. Prewitt, *Am. Mineral.* **2001**, 1483–1488.
[7] H. Yuan, H. Li, T. Zhang, G. Li, T. He, F. Du, S. Feng, *J. Mater. Chem. A* **2018**, 8413–8418.
[8] R. Albrecht, J. Hunger, T. Doert, M. Ruck, *Eur. J. Inorg. Chem.* **2019**, 1398–1405.
[9] W. M. Chance, D. E. Bugaris, A. S. Sefat, H.-C. zur Loye, *Inorg. Chem.* **2013**, *52*, 11723–11733.
[10] D. A. Pankratov, P. N. Komozin, Y. M. Kiselev, *Russ. J. Inorg. Chem.* **2011**, *56*, 1794–1799.
[11] K. Sardar, J. Fisher, D. Thompsett, M. R. Lees, G. J. Clarkson, J. Sloan, R. J. Kashtiban, R. I. Walton, *Chem. Sci.* **2011**, *2*, 1573–1578.
[12] B. B. Zvyagin, *Comput. Math. with Appl.* **1988**, *16*, 569–591.
[13] R. D. Shannon, *Acta Crystallogr. Sect. A* **1976**, *32*, 751–767.
[14] V. F. Sears, *Neutron News* **1992**, *3*, 26–37.
[15] J. M. Perez-Mato, S. V. Gallego, E. S. Tasci, L. Elcoro, G. de la Flor, M. I. Aroyo, *Annu. Rev. Mater. Res.* **2015**, *45*, 217–248.
[16] D. B. Litvin, *Acta Crystallogr. Sect. A* **2008**, *64*, 419–424.
[17] A. L. Hector, J. A. Hutchings, R. L. Needs, M. F. Thomas, M. T. Weller, *J. Mater. Chem.* **2001**, *11*, 527–532.
[18] L.-S. Xie, G.-X. Jin, L. He, G. E. W. Bauer, J. Barker, K. Xia, *Phys. Rev. B* **2017**, *95*, 014423.
[19] P. W. Anderson, *Phys. Rev.* **1950**, *79*, 350–356.
[20] J. B. Goodenough, *Phys. Rev.* **1955**, *100*, 564–573.
[21] J. Kanamori, *J. Phys. Chem. Solids* **1959**, *10*, 87–98.

[22] S. Ito, H. Kurosawa, K. Akashi, Y. Michiue, M. Watanabe, *Solid State Ionics* **1996**, *86*, 745–750.
[23] K. Kuwabara, T. Takahashi, *J. Appl. Electrochem.* **1977**, *7*, 339–343.
[24] G. McConohy, A. C. Baclig, A. D. Poletayev, J. Park, W. C. Chueh, *Solid State Ionics* **2019**, *337*, 82–90.
[25] S. Song, H. M. Duong, A. M. Korsunsky, N. Hu, L. Lu, *Sci. Rep.* **2016**, *6*, 1–10.
[26] D. Rettenwander, G. J. Redhammer, M. Guin, A. Benisek, H. Krüger, O. Guillon, M. Wilkening, F. Tietz, J. Fleig, *Chem. Mater.* **2018**, *30*, 1776–1781.
[27] *APEX2*, Bruker AXS Inc., Madison, Wisconsin, USA, **2014**.
[28] G. M. Sheldrick, *Sadabs: Area-Detector Absorption Correction*, Bruker AXS Inc., Madison, Wisconsin, USA, **2014**.
[29] G. M. Sheldrick, *Acta Crystallogr. Sect. A* **2015**, *71*, 3–8.
[30] G. M. Sheldrick, *Acta Crystallogr. Sect. C* **2015**, *71*, 3–8.
[31] K. Brandenburg, *Diamond 4, Crystal and Molecular Structure Visualization*, Crystal Impact GbR, Bonn, Germany, **2017**.
[32] A. Coelho, *Topas-Academic, v. 5*, Brisbane, Australia, **2012**.
[33] M. Hölzel, A. Senyshyn, R. Gilles, H. Boysen, H. Fuess, *Neutron News* **2007**, *18*, 23–26.
[34] M. Hölzel, A. Senyshyn, N. Jünke, H. Boysen, W. Schmahl, H. Fuess, *Nucl. Instrum. Methods Phys. Res. Sect. A* **2012**, *667*, 32–37.
[35] D. Richard, M. Ferrand, G. J. Kearley, *J. Neutron Res.* **1996**, *4*, 33–39.
[36] V. Petříček, M. Dušek, L. Palatinus, *Z. Kristallogr. – Cryst. Mater.* **2014**, *229*, 345–352.

Manuscript received: September 22, 2020
Revised manuscript received: October 27, 2020
Accepted manuscript online: October 29, 2020